Research Article

Ingo Rotscholl*, Klaus Trampert and Franz Schmidt

Spectral ray data for optical simulations

https://doi.org/10.1515/aot-2018-0049
Received September 28, 2018; accepted December 17, 2018; previously published online January 31, 2019

Abstract: This paper summarizes selected approaches, to generate spectral ray data for different types of spectrally varying light sources including only angular variable as well as spatial and angular variable sources. This includes a description of their general ideas and applications, the required measurements, and their mathematical concepts. Finally, achieved results for an Red/Green/Blue/White-light emitting diode (RGBW-LED) system are shown. Ray tracing simulations of a spatially and angularly spectral varying LED system combined with a spectrally sensitive optical system are qualitatively and quantitatively compared to a colorimetric far-field measurement of the same system. The results demonstrate the potential and benefits of spectral ray files in general.

Keywords: illumination design; light-emitting diodes; optical engineering; photometry; radiometry.

OCIS codes: 120.5240; 120.5630; 220.2945; 230.3670; 350.4600.

1 Introduction

Because of constant advances in the development of modern light sources and optical systems, the requirements in modern lighting industry are constantly growing. Modern high-quality lighting systems need to be, on the one hand, compact, highly efficient, smart, and color tunable and, on the other hand, appealing regarding their design and lighting distribution. This also includes aesthetic aspects such as uniformity and color uniformity. The complexity of designing high-quality lighting systems in an economically reasonable amount of time established the Monte Carlo ray tracing method as an important optical design tool [1].

In the Monte Carlo approach, a light source is represented as a large amount of rays, which can be defined as a measured ray file. A ray file can be interpreted as a stochastically discretized representation of the plenoptic function, ignoring the state of polarization. The plenoptic function is the most general light source description within the ray optic assumption [2]. Each ray file consists of a set of rays, where each ray is presented by a vector with a three-dimensional starting point and a two-dimensional direction [3].

Ray files can be measured using a near-field goniophotometer, as shown in Figure 1. It consists at least of a luminance camera (also called ILMD, imaging luminance measurement device) and two moving axes [5]. Because of a movement in angular space, the luminance camera provides angularly and spatially resolved luminance information of the light source. However, as the spectra are optically integrated on the electro optical sensor, a classic ray file does not contain spectrally resolved information. Often, a near-field goniophotometer includes a photometer for the absolute weighting of the radiant flux and a spectrometer. The spectrometer provides spectral information, which can also be angular resolved due to the goniometric movement but no spatially resolved spectral information.

In the Monte Carlo method, the rays are traced from the source through the optical system to the receiver according to the rules of geometrical optics. In addition to the geometrical information of the rays and the mechanics, the rules of geometrical optics require material parameters such as refractive indices or absorption coefficients, which are dependent on the wavelength. For this reason, the ray file needs to provide spectral information as well.

If analyzing the colorimetric or spectral distribution is not important, a monochromatic ray tracing is possible, and the light source description is given by the ray file. However, in the context of high-quality systems mentioned above, the inclusion of realistic spectral information is a critical aspect. Indeed, each error in the light source description will lead to deviations between the simulation and reality.

The color non-uniformities of modern lighting systems have two main origins. First, the spectral composition of light sources will, in general, vary angularly and spatially [3]. While this effect is negligible for classical tungsten

***Corresponding author: Ingo Rotscholl,** TechnoTeam Bildverarbeitung GmbH, Werner-von-Siemens-Strasse 5, 98693 Ilmenau, Germany, e-mail: ingo.rotscholl@technoteam.de
Klaus Trampert: Light Technology Institute, Karlsruhe Institute of Technology, Engesserstr. 13, 76131 Karlsruhe, Germany
Franz Schmidt: TechnoTeam Bildverarbeitung GmbH, Werner-von-Siemens-Strasse 5, 98693 Ilmenau, Germany

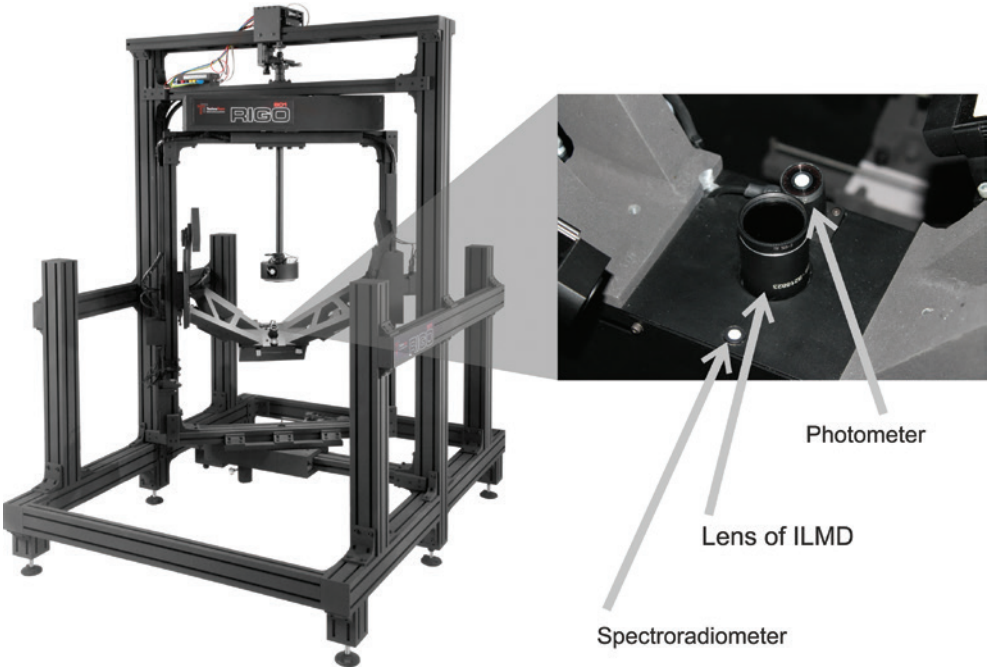

Figure 1: Example of a near-field goniophotometer (used under CC BY-SA 4.0 from Ref. [4]).

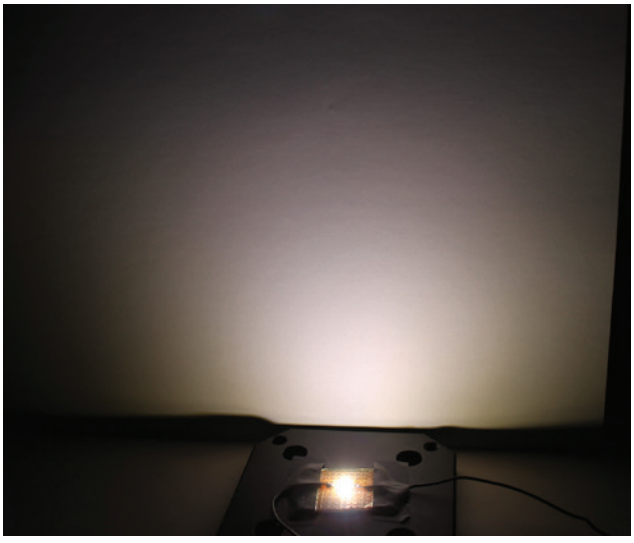

Figure 2: Typical color over angle deviation of a phosphor-converted white LED (used under CC BY-SA 4.0 from Ref. [4]).

Figure 3: Color non-uniformities of a head lamp (used under CC BY-SA 4.0 from Ref. [4]).

lamps, modern light sources such as LED systems can show much stronger variations. An example is provided in Figure 2, which shows a white LED with a typical color over angle variation.

Second, the applied optical elements such as lenses may be spectrally sensitive due to absorption or refraction and, thus, introduce chromatic effects as, for instance, the head lamp at the cut-off line shown in Figure 3. The consideration of both effects in the optical design process of high-quality lighting systems requires ray data, which includes angularly and spatially resolved spectral information [6, 7].

This paper will start with a brief summary of selected state-of-the-art methods to allocate spectral information to ray files. Here, only comparably fast methods, which only require a standard near-field goniophotometer, are considered. Afterward, it focuses on a recently developed method, which relies only on simple physical assumptions and is, thus, named 'Physically motivated basis spectra' or PMBS in short. To show the potential of spectral ray files, a spectral ray tracing simulation of a complex system,

namely, a Red/Green/Blue/White-light emitting diode (RGBW-LED) system, using spectral ray files created via the PMBS approach is compared to a colorimetric far-field measurement.

2 Generation of spectral ray data

To create spectral ray data, the five-dimensional measured ray data $M(x, y, z, \varphi, \vartheta)$ has to be extended to the six-dimensional $R(x, y, z, \vartheta, \varphi, \lambda)$ spectral ray file. This means at least a wavelength or a complete spectrum has to be assigned to each ray file. Depending on the complexity of the spectral distribution, the following different methods to create the spectral ray data can be applied.

2.1 Constant spectrum

For homogenous sources, like a tungsten lamp, the spectrum does not depend on the angular or spatial dimension. In this case, the task is straightforward. One measured global spectrum $S_{\text{global}}(\lambda)$ can serve as probability density functions for all rays equally such that Equation (1) applies

$$R(x, y, z, \vartheta, \varphi, \lambda) = M(x, y, z, \varphi, \vartheta) \times S_{\text{global}}(\lambda) \tag{1}$$

However, for modern sources, the spectral variation is often a function of the angular and spatial dimension. Then, Equation (1) is not sufficient.

2.2 Angle-dependent spectra

If only angular spectral variations are relevant and spatial variations can be neglected, as in the case of organic light emitting diode, the PCA (principal component analysis) approach from Refs. [8] and [9] can be used. Besides a conventional ray file measurement, this approach requires angular resolved spectral measurements to obtain the angularly varying spectral information $S(\vartheta, \varphi, \lambda)$. Then, a PCA is performed to obtain a set of (mathematical) basis spectra $S_{\text{PCA},n}(\lambda)$ and angular resolved weighting factors $w_n(\vartheta, \varphi)$ for each measured position. It applies that

$$S(\vartheta, \varphi, \lambda) = \sum_{n=1}^{m} w(\vartheta, \varphi)_n \times S_{\text{PCA},n}(\lambda), \tag{2}$$

With these data, it is possible to interpolate the complete spectrum at all other angular positions $\tilde{S}(\vartheta, \varphi, \lambda)$. Based on the measured ray file $M(x, y, z, \varphi, \vartheta)$ and the interpolated spectra $\tilde{S}(\vartheta, \varphi, \lambda)$, an overall weighting $\tilde{k}(\vartheta, \varphi)$ can be derived for each direction such that the final spectral ray file is defined as

$$R(x, y, z, \vartheta, \varphi, \lambda) = M(x, y, z, \varphi, \vartheta) \times \tilde{k}(\vartheta, \varphi) \times \tilde{S}(\vartheta, \varphi, \lambda) \tag{3}$$

2.3 Spatial and angle-dependent spectra

There are also methods [4, 10–12], which are capable of including spatial and angular resolved spectral variations. The main idea is to combine several ray files such that each different ray file $M_n(x, y, z, \varphi, \vartheta)$ is assigned to a different spectrum

$$R(x, y, z, \vartheta, \varphi, \lambda) = \sum_{n=1}^{n_{\max}} M_n(x, y, z, \varphi, \vartheta) \times S_{\text{Base},n}(\lambda), \tag{4}$$

$$\text{With } S_{\text{global}}(\lambda) = \sum_{n=1}^{n_{\max}} S_{\text{Base},n}(\lambda). \tag{5}$$

An advantage of these methods is that the recently standardized ray file format TM25-13 can be applied to these types of models [13]. A well-known and common procedure is the Blue/Yellow approach [10]. It addresses the spectral ray file creation problem specifically for phosphor-converted white LEDs. In this model, one ray file describes the blue LED and the other the yellow phosphor such that $n_{\max} = 2$. Both ray files are measured using different optical filters to separate the spectral parts during the two ILMD-based goniometric measurements.

Currently, the needed basis spectra in this approach are deduced from one global spectrum by a sharp spectral separation at a cut wavelength:

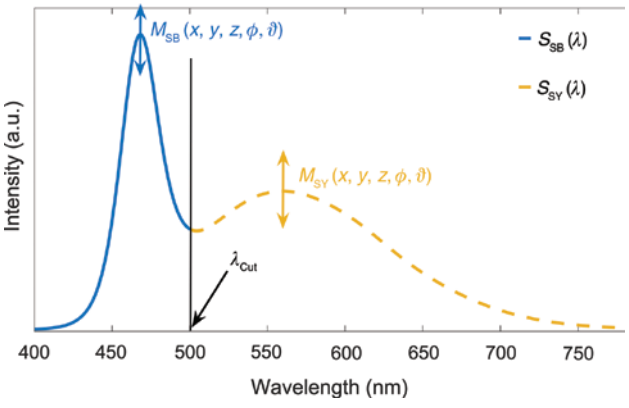

Figure 4: Exemplarily, sharp separated basis spectra in the blue/yellow approach (used under CC BY-SA 4.0 from Ref. [4]).

$$S_{\mathrm{Base},n}(\lambda)=\begin{cases}0 & \lambda<\lambda_{\mathrm{Cut},n-1}\\ S_{\mathrm{global}}(\lambda) & \lambda_{\mathrm{Cut},n-1}\le\lambda<\lambda_{\mathrm{Cut},n}\\ 0 & \lambda_{\mathrm{Cut},n}\le\lambda<\infty\end{cases}, \tag{6}$$

Figure 4 shows this basis spectra concept. However, this artificial sharp separation introduces a systematic error because the real physical spectra differ from the defined basis spectra in Figure 4. As this method is used for phosphor-converted white LEDs in the industry, it can be assumed that this systematic error is tolerable for these LED spectra. However, it becomes too large in the case of complex LED systems. Therefore, this approach is limited to phosphor-converted white LED only. A comparison for a specific example is provided in Ref. [14]

A more general procedure for LEDs is the recently described PMBS approach, which combines ideas from the PCA and the Blue/Yellow approach [4]. It will be discussed briefly in the next sub section.

2.4 Physically motivated basis spectra

The main assumption of the PMBS approach is that each spatial and angle-dependent spectral variation can be described as the weighted sum of its physically occurring basis spectra. The basis spectra $S_{\mathrm{Base},n}(\lambda)$ are the spectra of the different spectral sources, like semiconductors and phosphors. The weighting factors $A_n(x, y, z, \varphi, \vartheta)$ determine their relations as a function of angular and spatial dimension.

$$R(x, y, z, \vartheta, \varphi, \lambda)=\sum_{n=1}^{n_{\max}}A_n(x, y, z, \varphi, \vartheta)\times S_{\mathrm{Base},n}(\lambda), \tag{7}$$

Equation (7) looks very similar to Equation (4). The main difference is that the distributions $A_n(x, y, z, \varphi, \vartheta)\neq M_n(x, y, z, \varphi, \vartheta)$, which means that the distribution $A_n(x, y, z, \varphi, \vartheta)$ can, in general, not be measured directly and that the basis spectra $S_{\mathrm{Base},n}(\lambda)$ directly represent a physical source. This is indicated by a comparison of Figure 5 to Figure 4. While in Figure 4 the basis spectra are more artificial, Figure 5 provides more realistic basis spectra of the individual physical components.

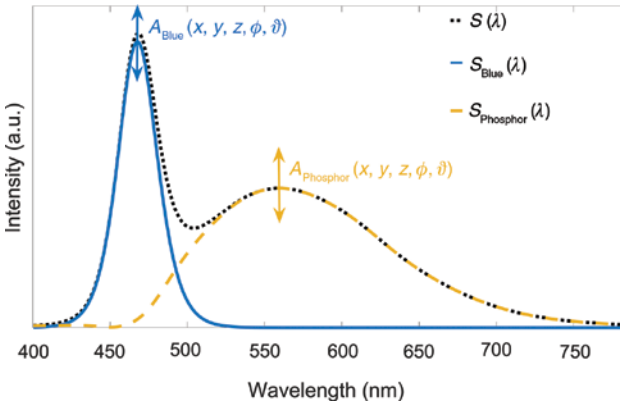

Figure 5: Exemplarily, physical basis spectra of a phosphor-converted white LED according to the PMBS approach (used under CC BY-SA 4.0 from Ref. [4]).

By applying the light source model from Equation (7) to an ILMD measurement, the relation between the angularly and spatially resolved measurement result $M(x, y, z, \varphi, \vartheta)$ and the actual physical amplitude distributions $A_n(x, y, z, \varphi, \vartheta)$ is given by

$$M(x, y, z, \varphi, \vartheta)=\sum_{n=1}^{n_{\max}}A_n(x, y, z, \varphi, \vartheta)\times\int S_{\mathrm{Base},n}(\lambda)\times\tau(\lambda)\times s_{\mathrm{sys}}(\lambda)d\lambda, \tag{8}$$

where $\tau(\lambda)$ is a changeable transmission function of the ILMD optical system including neutral density filters. The variable $s_{\mathrm{sys}}(\lambda)$ is the constant spectral sensitivity of the system including the electro optical sensor and the lens transmission. If the transmission $\tau(\lambda)$ in Equation (8) changes, for instance because different transmission filters are applied, the generated measurement result will change as well. The idea of the PMBS approach is to combine at least $n_{\max}$ ILMD-based goniometric measurements with different selected filter transmissions $\tau_n(\lambda)$ to reconstruct the unknown amplitude distributions by solving the resulting system of linear equations as defined by Equation (9).

$$\begin{bmatrix}A_1(x, y, z, \varphi, \vartheta)\\ \vdots\\ A_{n_{\max}}(x, y, z, \varphi, \vartheta)\end{bmatrix}=M_{s\tau}^{-1}\cdot\begin{bmatrix}M_1(x, y, z, \varphi, \vartheta)\\ \vdots\\ M_{n_{\max}}(x, y, z, \varphi, \vartheta)\end{bmatrix}$$

with

$$M_{s\tau}=\begin{bmatrix}\int S_{\mathrm{Base},1}(\lambda)\times\tau_1(\lambda)\times s_{\mathrm{sys}}(\lambda)d\lambda & \cdots & \int S_{\mathrm{Base},n_{\max}}(\lambda)\times\tau_1(\lambda)\times s_{\mathrm{sys}}(\lambda)d\lambda\\ \vdots & \ddots & \vdots\\ \int S_{\mathrm{Base},1}(\lambda)\times\tau_{n_{\max}}(\lambda)\times s_{\mathrm{sys}}(\lambda)d\lambda & \cdots & \int S_{\mathrm{Base},n_{\max}}(\lambda)\times\tau_{n_{\max}}(\lambda)\times s_{\mathrm{sys}}(\lambda)d\lambda\end{bmatrix} \tag{9}$$

Equation (9) is called the reconstruction equation. The reconstruction uses both the derived physical basis spectra $S_{\mathrm{Base},n}(\lambda)$ and a description of the spectral sensitivity of the ILMD $\tau_n(\lambda) \cdot s_{\mathrm{sys}}(\lambda)$ in the measurement setup. If the basis spectra are known, the distributions $A_n(x, y, z, \varphi, \vartheta)$ can be reconstructed. Then they can be combined with each other and the basis spectra according to Equation (7) to get the spectral ray file.

In order to practically apply the approach, the workflow shown in Figure 6 can be used. First, the basis spectra of the measurement object need to be estimated. This can be performed using the spectrometer from a near-field goniophotometer. It is best practice to measure each basis spectrum individually if possible. If this is not possible, they can be estimated out of an integrated spectrum, which is the more complex case. Based on received basis spectra, an optimized filter set $\tau_i(\lambda)$ can be selected. In the third step, the $n_{\max}$ near-field goniophotometer measurements have to be carried out while applying the selected filters on the ILMD. Finally, the spectral information of the ILMD $\tau(\lambda) \cdot s_{\mathrm{sys}}(\lambda)$, the basis spectra $S_{\mathrm{Base},n}(\lambda)$, and the $n_{\max}$ measured ray files $M(x, y, z, \varphi, \vartheta)$ can be used to create the distribution of the spectral ray files, which can each be assigned to one of the estimated basis spectra.

Further, an optional additional basis spectra optimization can be performed. This optimization utilizes the knowledge that individual LED chips including difference LED colors are spatially separated and highly localized in the three-dimensional space. A more detailed description of the overall process including several step-by-step examples are provided in Ref. [4]. The filter selection process and the application of the reconstruction equation on ray files are explained in Refs. [15] and [16]. This includes discussions of the influence of uncertainties within the measurement setup as well as the influence of the initial resolution of the measured ray files.

The PMBS approach cannot include nonlinear effects, such as phosphor self absorption or quenching. The same is true for chromatic aberrations, which are caused by primary optics. If these effects are relevant or dominant, PMBS should not be used. In the case of phosphor-converted white LEDs, the influence of such effects can be estimated via angularly resolved colorimetric measurements. If the measured chromaticities are on a straight line in the CIE *xy* or CIE *u′v′* diagram, then the linear assumption of PMBS is valid because the additive color mixing changes the chromaticity only between the chromaticity coordinate of the blue LED and the chromaticity coordinate of the yellow phosphor [4].

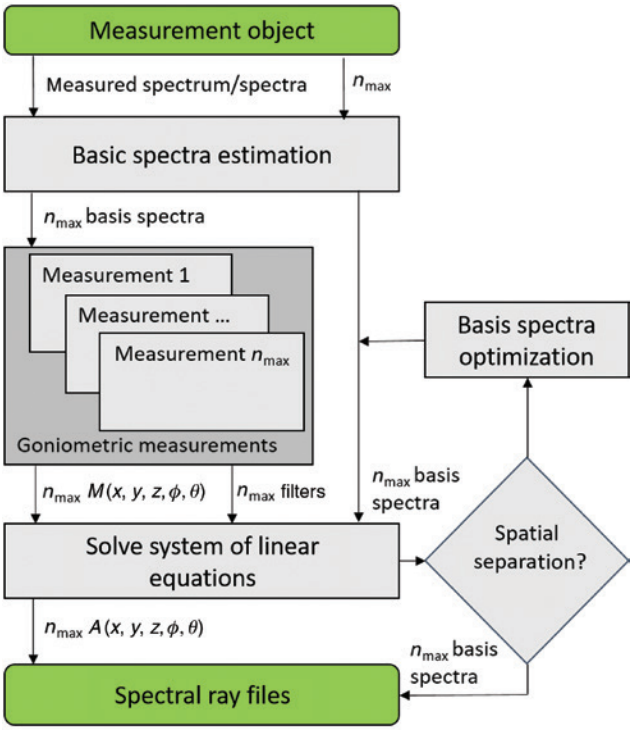

Figure 6: Practical workflow to apply PMBS (slightly changed under CC BY-SA 4.0 from Ref. [4]).

3 Spectral ray data in optical simulations

In order to show the capability of spectral ray files, an example generated with the PMBS approach is used in the commercial ray tracer OptisWorks (OPTIS, France) to simulate a colorimetric distribution of a RGBW-LED system in combination with a dispersion prism. The dispersion prism was chosen because it is, on the one hand, a spectrally sensitive system and, on the other hand, a simple geometric object. Thus, the deviations between the real object and its virtual representation are expected to be low.

Figure 7 visualizes the RGBW-LED system used for the experiment. It was first introduced in Ref. [17] and consists of five RGBW-LEDs with one RGBW-LEDs in the middle and one in each corner. The visualized apertures ensure that the different colors are clearly separated in the near field but start to mix in the far field. This enables a more precise assessing of the reconstruction but still leads to complex color non-uniformities.

This complex configuration is chosen because, in this case, the optional basis spectra optimization does improve the result significantly. The number of fundamental different basis spectra is four because we assume that the blue basis spectrum of the blue LED chip and the blue spectrum of the white LED do not deviate significantly from each

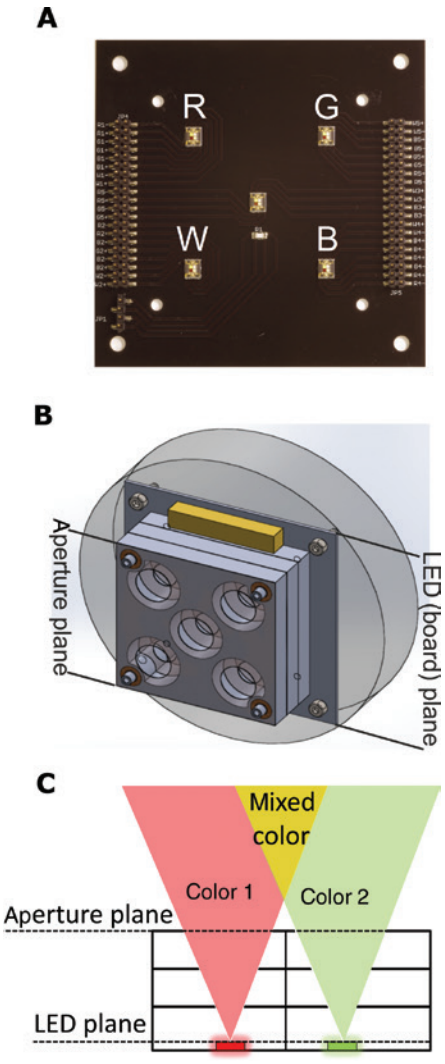

Figure 7: Measurement object used: (A) LED board and its configuration; (B) housing with apertures, and (C) principle of color mixture (used under CC BY-SA 4.0 from Ref. [4]).

other. This assumption bases on a comparison of the LED spectra according to their datasheet specifications. Note that, the overall quality of the spectral description, which includes the transmissions and spectral sensitivities of the measurement system and the basis spectra modeling can be estimated by exemplary reconstructions (see also the appendix) or additional spectral reference measurements on the goniometer and punctual spectral reconstruction on this reference measurement positions [4].

Thus, altogether, four goniometric measurements with a RIGO801 near-field goniophotometer (TechnoTeam, Germany), which was equipped with an ILMD (LMK5-5 color, TechnoTeam, Germany), were performed. The basis spectra estimation of this validation bases on only one spectral measurement. It was performed with the spectrometer (specobs1211, JETI, Germany) from the near-field goniophotometer. We use only one measured spectrum for this experiment to test a worst-case scenario, in which individual spectral measurements of the basis spectra are not possible. A step by step reconstruction of this example is provided in the appendix.

To perform a ray tracing simulation using the spectral ray file, the four derived distributions $A_{1\text{–}4}(x, y, z, \varphi, \vartheta)$ were represented as ray files (10 million rays for each ray file) and assigned to their respective basis spectra $S_{\text{Base},1\text{–}4}(\lambda)$, which had a resolution of 0.25 nm. Then, each ray file is directly loaded into the ray tracer. The basis spectra serve as probability density functions, which statistically assigns a wavelength to each ray of the spectral ray file. The overall flux of each spectral ray file is calculated with PMBS and the camera luminous fluxes as described in Ref. [4]. Within the ray tracer, the spectral resolution of the sensor was 1 nm between 380 nm and 780 nm.

The ray tracing simulation is compared to a conventional high resolved far-field measurement of the optical system using an automotive goniometer GO-H 1660 (LMT, Germany) equipped with a colorimeter C3300 (LMT,

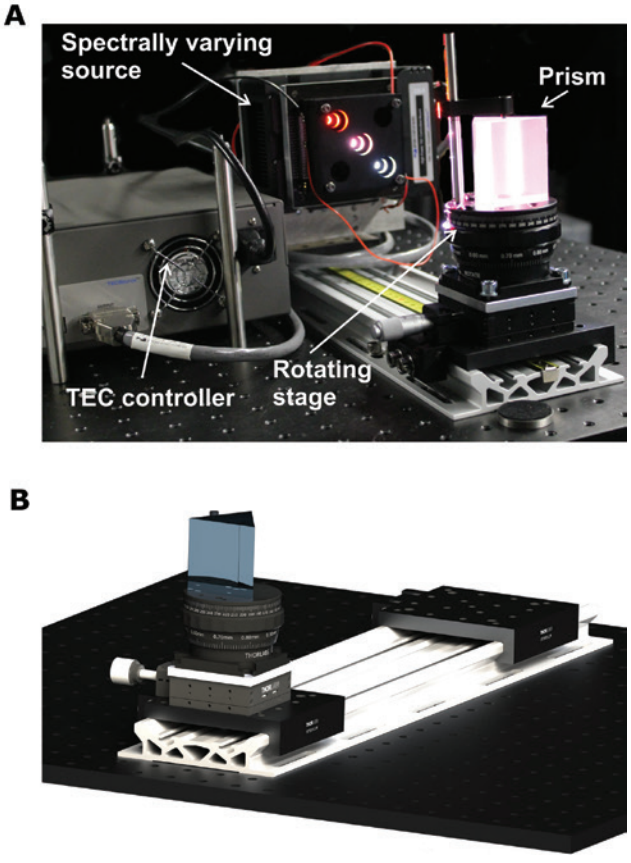

Figure 8: (A) Experimental setup of far-field measurement and (B) setup in spectral ray tracing simulation (used under CC BY-SA 4.0 from Ref. [4]).

Germany). Figure 8 shows the experimental setup as well as the simulation setup in OptisWorks. An optical bench with rotating plate and special holder was used for the geometrical alignment in the real and the virtual setup to align the experiment and simulation.

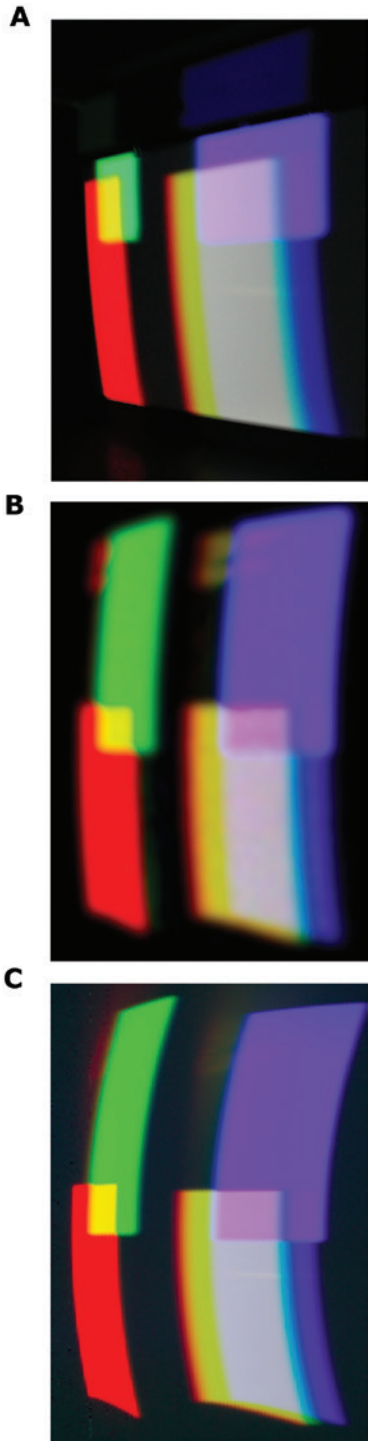

Figure 9: (A) Photographic image of distribution during measurement. (B) Distribution according to colorimetric measurement transformed to RGB. (C) Resulting distribution of spectral ray tracing transformed to RGB (used under CC BY-SA 4.0 from Ref. [4]).

Figure 9 shows a qualitative comparison of the distribution. Figure 9A is a photographic image, which was taken with a commercial consumer camera as reference for the overall distribution (A). The overall distribution consists of four sub distributions (red, green, blue, and white), which can each be assigned to an individual corner of the measurement object (see Figure 7A). They partly overlap and, thus, create additional mixture regions, as for instance the yellow region. Further, there is a clear dispersion effect on each distribution, which is strongest for the white distribution.

Figure 9B shows the result of the far-field measurement. The RGB values were converted from directly measured tristimulus values obtained via the C3300. Figure 9C visualized the result of the spectral ray tracing simulation. The spectral ray files were calculated using PMBS on the four measured ray files. They were traced toward a spectrally resolved intensity sensor with a resolution of 1 nm. Thus, the spectrum at each interval of the intensity sensor was simulated. For comparison, the spectral resolved intensity information was converted to tristimulus values and RGB values. In Figure 9B and C, the photometric center was the dispersion prism. The general reference picture (A) was taken from a different perspective. The relative shape and color of the simulated (C) and measured distribution (B) show a very good agreement. This includes reflections, as the red spot and yellow spots in the upper regions.

However, a more detailed comparison reveals some deviations in the shape. The first deviation is the curvature of the colored distributions especially on the right-hand side. The second deviation is the relative position of each sub distribution, which can be seen by the relative location of the green distribution.

It is important to ensure that these deviations are not an artifact caused by the generation of the spectral ray files. A way to ensure this is to compare the shape of a ray tracing simulation using the original measured ray files to the shape of a ray tracing simulation using the deduced spectral ray files. The shape of the simulation using the original ray files serves as ground truth reference. However, it has to be taken into account that the effect of the dispersion prism on the shape is not considered correctly in the reference simulation because there is no spectral information available. To only compare the relative distributions, the spectral ray files and the original ray files are traced with the same monochromatic wavelength. This comparison is shown in Figure 10.

As the shapes in Figure 10A and B are identical, it can be concluded that the deviations do not occur due to the generation of the spectral ray files and are likely to be

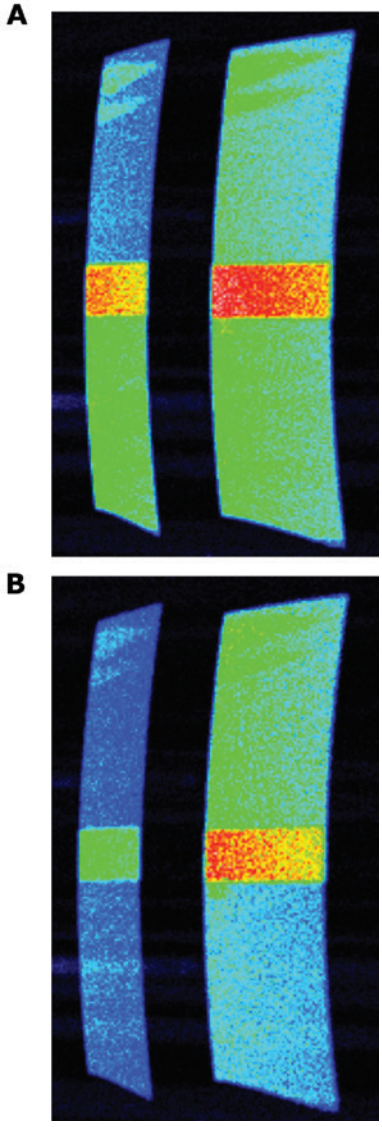

Figure 10: Comparison of shape obtained from ray tracing using originally measured ray files (A) and ray files from PMBS (B) (used under CC BY-SA 4.0 from Ref. [4]).

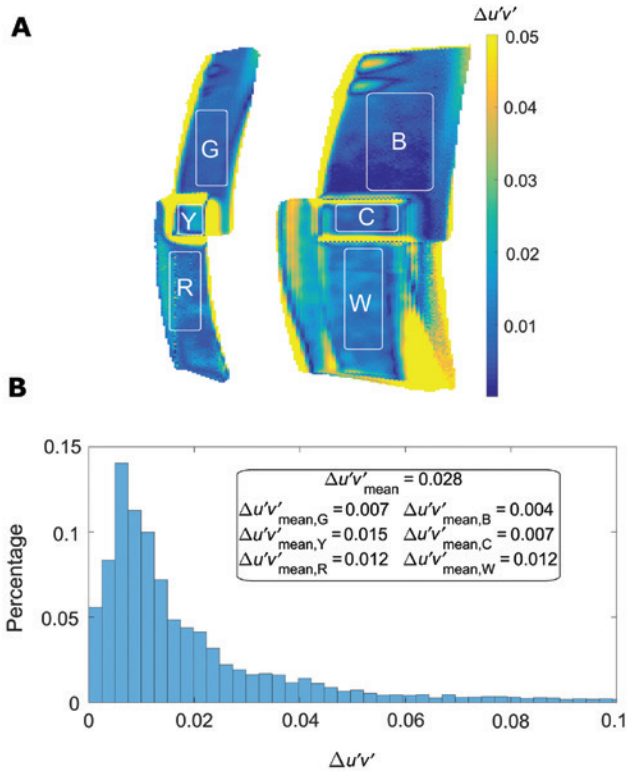

Figure 11: Quantitative comparison of spectral ray tracing simulation and colorimetric far-field measurement: (A) pixel-wise and (B) histogram (used under CC BY-SA 4.0 from Ref. [4]).

caused by a difference of the positioning of light source and prism between the far-field measurement and the simulation. To support this assumption, we performed additional ray tracing simulations with slightly adjusted alignments. As expected, the simulation revealed a high sensitivity of the alignment on the final shape of the distribution for the setup of this experiment.

The imperfect alignment has to be considered during a quantitative comparison as well. Figure 11 shows the chromaticity coordinate distance $\Delta u'v'$ between the measured and simulated chromaticity coordinates as a function of the spatial dimension as well as histogram.

The high deviations at the edges occur mainly due to the misalignment between the simulation and the measurement. Therefore, the mean deviation of the six evaluation regions R, G, B, W, Y, and C are more meaningful than the maximal values. The mean deviation are between $\Delta u'v' = 4 \times 10^{-3}$ and 1.2×10^{-2} for the spectral pure regions R, G, and B and between $\Delta u'v' = 1.2 \times 10^{-2}$ and 1.5×10^{-2} for the mixed regions W, Y, and C. Further, an analysis of the individual chromaticity differences shows that large parts of these deviations are caused by an offset. In this case, the results of a uniformity analysis, which analyzes relative deviations within the distribution, would be less affected.

Further, there is a significant difference in the shape between the monochromatic ray file simulations in Figure 10 and the spectral ray file simulation in Figure 9B. As the spectral ray file simulation shows a better agreement to the measured (and photographed) distribution, it can be concluded that applying a spectral ray file does not only allow to evaluate colorimetric and spectral properties but also to improve classical geometric and photometric evaluations.

4 Conclusions

This paper provides a brief overview of selected, practical possibilities to generate spectral ray data for optical

simulations in order to develop high-quality lighting systems. Depending on the angular and spatial variations of the light source spectra, different procedures as a global spectrum, angular weighted principal components of spectra (PCA) or angularly and spatially weighted physical-derived basis spectra (PMBS) can be assigned to the ray file(s).

Further, the capabilities of spectral ray files were shown on a complex spectral system by comparing the colorimetric far-field distribution with a ray tracing simulation based on spectral ray file created via the shown PMBS approach. The so generated spectral ray files allowed a more precise simulation of the spectrally sensitive systems by considering the spatial and angular spectral information of the source. The simulation with the spectral ray file did not only add colorimetric/spectral information but also improved the agreement between the geometrical shape of the measured distribution compared to a monochromatic simulation.

The deviations, which occur between experiment and simulation, are within the color discrimination thresholds in practical applications according to Ref. [18] and are mainly caused by misalignment and measurement uncertainties between the different measurement instruments for the far field and the near field, including ILMD, spectrometer, and colorimeter. As the largest part of these deviations are caused by an offset, the relative deviations required for a uniformity analysis are even lower.

Further, it shall be mentioned that this paper presents the most critical reconstruction performed with PMBS so far. The colorimetric deviations for a simpler system, as for instance phosphor-converted white LED, are less sensitive and in the order of $\Delta u'v' = 2 \times 10^{-3}$ [4], which is near the region of the uncertainty of the used measurement instruments. Therefore, it can be concluded that there are methods to create spectral ray files, which can be used to improve the optical design of high-quality LED-based lighting systems with respect to photometric, colorimetric, and spectral evaluations.

Appendix

This appendix explains the application of PMBS to obtain the spectral ray files of the example discussed in this paper in more detail. An even more detailed description and more examples are provided in Ref. [4].

The first step is the initial basis spectra estimation, which bases on one spectral measurement at main radiance direction. All basis spectra overlapped at the chosen measurement distance.

Figure 12 shows the estimated parametrized basis spectra blue $S_1(\lambda, x)$, red $S_2(\lambda, x)$, green $S_3(\lambda, x)$, and phosphor $S_P(\lambda)$ and compare them to parametrized fits of the basis spectra derived from individual measurements for reference. The resolution of each spectral measurement was 1 nm with a bandwidth of 5 nm. Note that the phosphor reference was derived from a measurement of only the white LED in the lower left corner. While the red and blue basis spectra estimation is very precise, there are slight deviations in the case of the phosphor spectrum and the green LED spectrum due to their large spectral overlap.

However, these spectra are sufficient to choose an appropriate set of filter transmission functions from the standard filters as well as the glass absorption filters

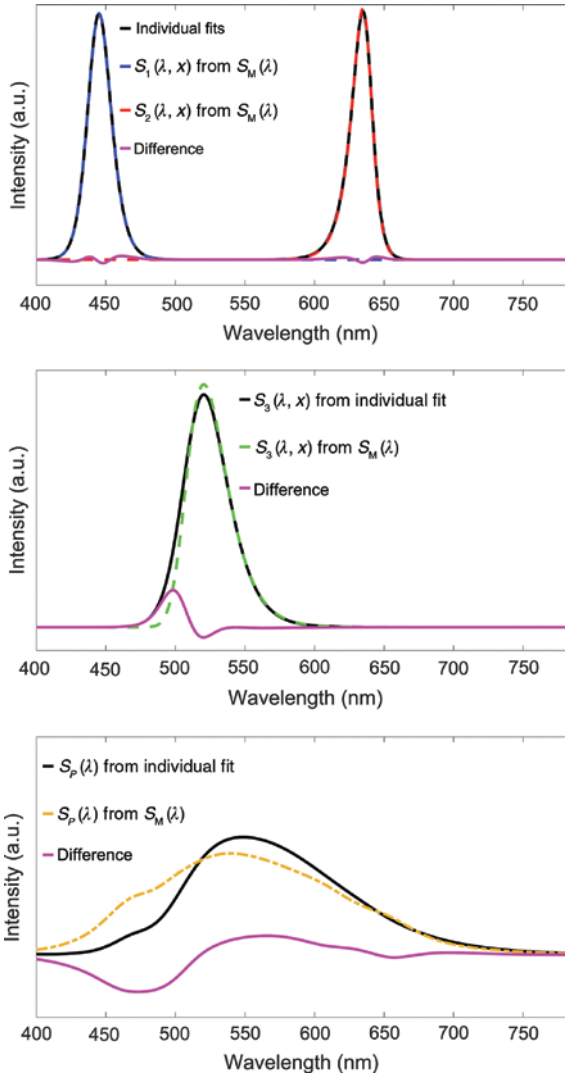

Figure 12: Basis spectra after initial estimation (used under CC BY-SA 4.0 from Ref. [4]).

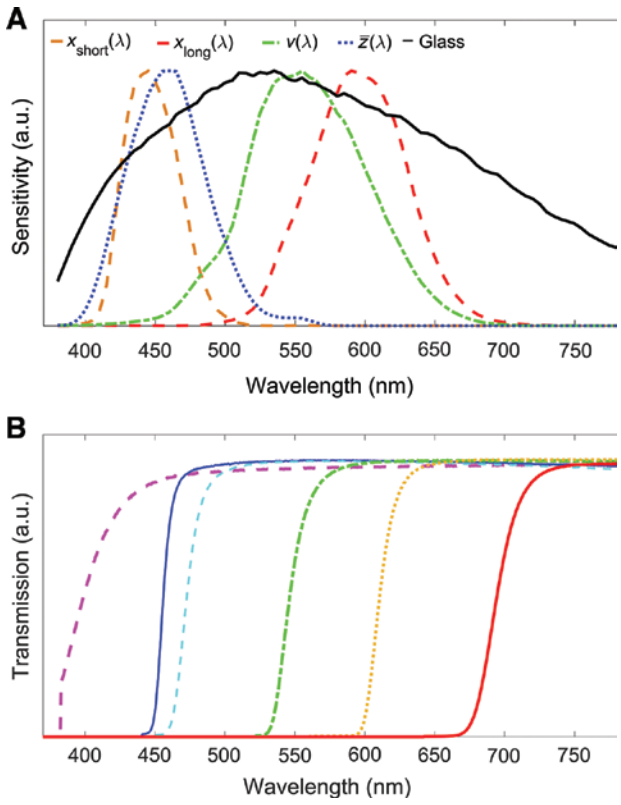

Figure 13: Spectral sensitivity of system with standard filters (A) and transmission of additional glass absorption filters for a combination with the glass standard filter sensitivity (B) (used under CC BY-SA 4.0 from Ref. [4]).

shown in Figure 13A and B. Figure 14 shows the four measured ray files using the selected filter set as irradiances in the aperture plane. The angular resolution of each near-field measurement was set to 0.5 deg for both angular dimensions. Each ray file consists of 10 million equally weighted rays. The near-field information is provided by the spatial and angular density of the rays. The numbers above the irradiances in Figure 14 identify the selected glass absorption filters and equal the edge wavelength, where the internal transmission equals 50%.

By utilizing the spectral information from Figures 12 and 13 as well as the projected irradiances in Figure 14, the irradiances of the reconstruction can be estimated and assessed with respect to their spatial separation and their degree of localization [4]. The reconstruction is shown in Figure 15.

While the delocalization of the blue reconstruction occurs because there are two blue LED chips in the system, the delocalization of the red and especially the green LED is a reconstruction artifact. These artifacts can occur due to uncertainties of the spectral transmissions and the basis spectra description.

Finally, the basis spectra can be optimized with respect to the spatial separation and the degree of localization as described above. Figure 16 visualizes the resulting basis spectra and their projected irradiances. They show a clear improvement if they are compared to the reference spectra.

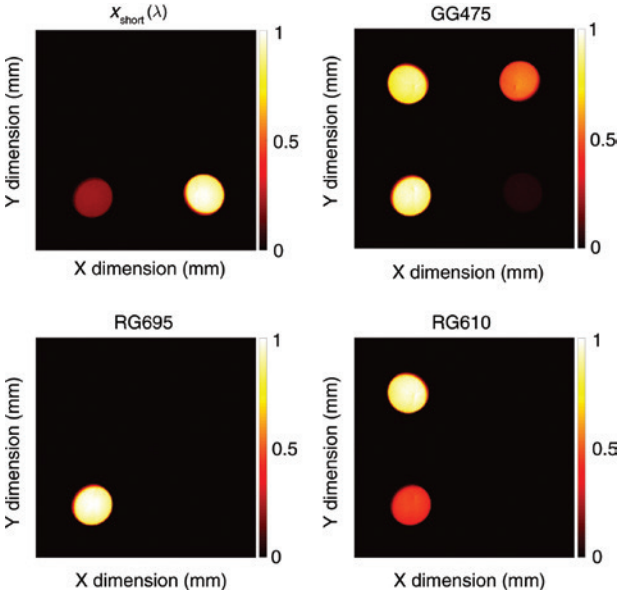

Figure 14: Measured ray files using the x_{short} filter wheel position and the glass filter wheel position in combination with the absorption filters GG475, RG610, and RG695 from Ref. [19] (used under CC BY-SA 4.0 from Ref. [4]).

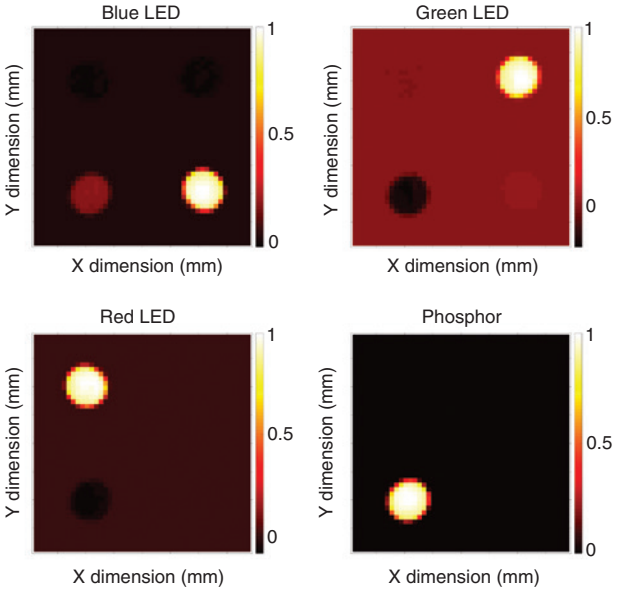

Figure 15: Estimated reconstruction as irradiance in the aperture plane using initially estimated basis spectra (used under CC BY-SA 4.0 from Ref. [4]).

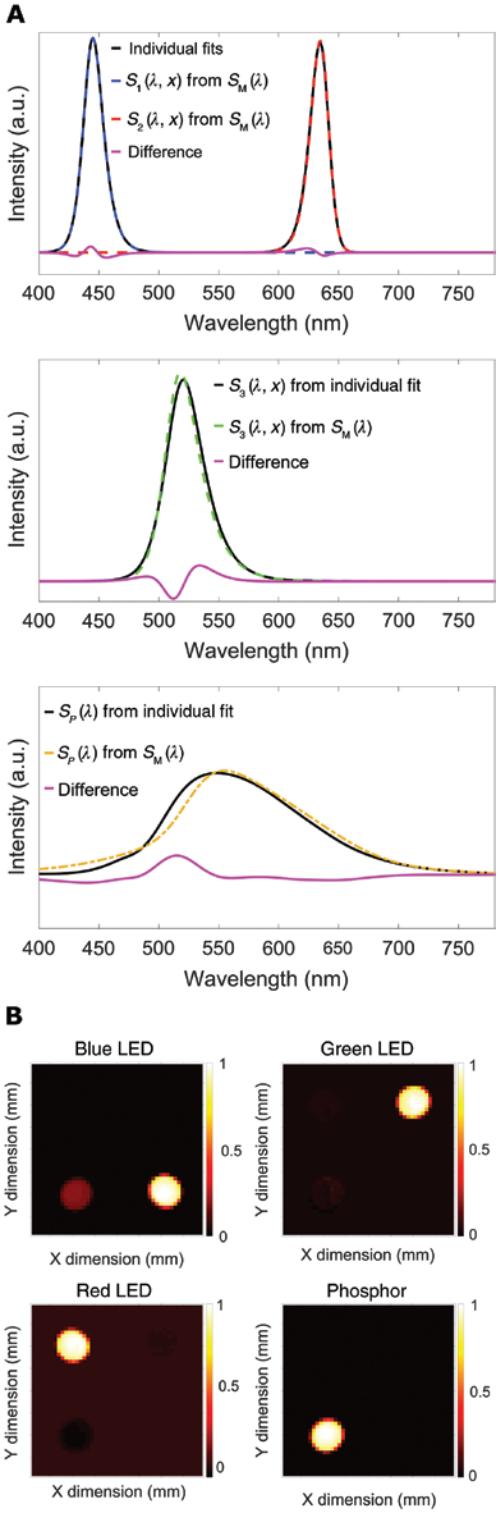

Figure 16: (A) Basis spectra after basis spectra optimization and (B) achieved reconstruction as irradiance in the aperture plane using optimized basis spectra (used under CC BY-SA 4.0 from Ref. [4]).

Especially, the phosphor spectrum changed significantly, which also reduced the reconstruction artifacts in the projected irradiances. Finally, the spectral ray file can be created utilizing the procedure described in Refs. [4] and [16].

Acknowledgments: This work was supported by the Federal Ministry of Education and Research in the Program Photonics Research Germany (Funder Id: 10.13039/501100002347, contract number 13N13396).

References

[1] H.-J. J. Frasch and G. Steinmetz, Proc. SPIE 4769, 54–66 (2002).
[2] E. H. Adelson and J. R. Bergen, in 'Computational Models of Visual Processing', (Vision and Modeling Group, Cambridge, MA, USA, 1991).
[3] R. Dürr and U. Streppel, in 'Proceedings of the International Light Simulation Symposium', Nuremberg, 2012.
[4] I. Rotscholl, 'Spectral Near Field Data of LED Systems for Optical Simulation', (KIT Scientific Publishing, Karlsruhe, 2018), http://dx.doi.org/10.5445/KSP/1000078518.
[5] I. Ashdown, J. Illum. Eng. Soc. 22, 163–180 (1993).
[6] J. Nevoigt, in 'Licht', 2018, (Schweizer Licht Gesellschaft, Davos, 2018).
[7] G. Durinck, F. B. Leloup, J. Audenaert and P. Hanselaer, Light Eng. 25, 103–112 (2017).
[8] V.-A. Jacobs, J. Audenaert, J. Bleumers, G. Durinck, P. Rombauts et al., Opt. Express 23, A361–A370 (2015).
[9] V. Jacobs, J. Audenaert, J. Bleumers, G. Durinck, P. Rombauts, et al., 'On spectral ray files of light sources using principal component analysis', in Proceedings of 28th CIE Session (CIE, 2015), 543–547.
[10] OSRAM Opto Semiconductors GmbH, 'Application Note: Importing Rayfiles of LED from OSRAM Opto Semiconductors', (2013).
[11] D. Hansen, S. Paul and V. Schumacher, in 'LED Professional Symposium', (2012).
[12] R. Rykowsky, Light Eng. 19, 23–29 (2011).
[13] Illuminating Engineering Society, 'IES TM25-13 Ray File Format for the Description of the Emission Property of Light Sources', (2013).
[14] I. Rotscholl, K. Trampert, U. Krüger, I. Saynca, F. Schmidt, et al., LED Prof. Rev. 63, 48–56 (2017).
[15] I. Rotscholl, K. Trampert, U. Krüger, M. Perner, F. Schmidt, et al., Opt. Express 23, 29543–29554 (2015).
[16] I. Rotscholl, M. Katona, K. Trampert, U. Krüger, F. Schmidt, et al., Opt. Express 24, A1597–A1611 (2016).
[17] I. Saynca, K. Trampert and C. Neumann, in 'Proceedings of the Lux Junior', Dörnfeld/Ilm, 2017.
[18] K. Bieske and T. Fiebig, in 'Licht', 2014, (NSVV, Den Haag, 2014).
[19] A. G. Schott, in 'Optical Filters', (2014), https://www.schott.com/d/advanced_optics/a81cd277-746f-499d-90d2-38724bd120e5/1.1/schott-optical-filters-2014-catalog-complete-en.pdf (Accessed July 2015).